Journal of Hazardous Materials 351 (2018) 301–307

Contents lists available at ScienceDirect

Journal of Hazardous Materials

journal homepage: www.elsevier.com/locate/jhazmat

# Research of mercury removal from sintering flue gas of iron and steel by the open metal site of Mil-101(Cr)

Songjian Zhao[a,b], Jian Mei[a], Haomiao Xu[a], Wei Liu[a], Zan Qu[a], Yong Cui[b], Naiqiang Yan[a,*]

[a] School of Environmental Science and Engineering, Shanghai Jiao Tong University, 800 Dong Chuan Road, Shanghai, 200240, PR China
[b] School of Chemistry and Chemical Engineering, Shanghai Jiao Tong University, 800 Dong Chuan Road, Shanghai, 200240, PR China

## HIGHLIGHTS

- Metal-organic frameworks adsorbent Mil-101(Cr) was introduced for $Hg^0$ removal.
- Mil-101(Cr) has a higher $Hg^0$ removal efficiency compared with UiO-66 and Cu-BTC.
- The open metal site of Mil-101(Cr) was important for $Hg^0$ removal.

## GRAPHICAL ABSTRACT

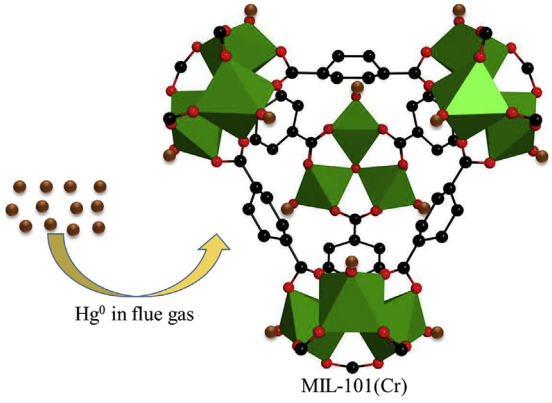


$Hg^0$ removal in flue gas by the open metal site of Mil-101(Cr)

## ARTICLE INFO

*Article history:*
Received 7 August 2017
Received in revised form 5 November 2017
Accepted 6 December 2017
Available online 7 December 2017

*Keywords:*
Mil-101(Cr)
Adsorbent
Mercury
Removal

## ABSTRACT

Metal-organic frameworks (MOFs) adsorbent Mil-101(Cr) was introduced for the removal of elemental mercury from sintering flue gas. Physical and chemical characterization of the adsorbents showed that MIL-101(Cr) had the largest BET surface area, high thermal stability and oxidation capacity. $Hg^0$ removal performance analysis indicated that the $Hg^0$ removal efficiency of MIL-101(Cr) increased with the increasing temperature and oxygen content. Besides, MIL-101(Cr) had the highest $Hg^0$ removal performance compared with Cu-BTC, UiO-66 and activated carbon, which can reach about 88% at 250 °C. The XPS and Hg-TPD methods were used to analyze the $Hg^0$ removal mechanism; the results show that $Hg^0$ was first adsorbed on the surface of Mil-101(Cr), and then oxidized by the open metal site $Cr^{3+}$. The generated $Hg^{2+}$ was then combined surface adsorbed oxygen of adsorbent to form HgO, and the open metal site $Cr^{2+}$ was oxidized to $Cr^{3+}$ by surface active oxygen again. Furthermore, MIL-101(Cr) had good chemical and thermal stability.



## 1. Introduction

Mercury was listed as a hazardous and toxic pollutant under Title III of the 1990 Clean Air Act Amendments (CAAA) in the United States [1]. In recent years, environmental pollution with mercury has attracted increasing attention due to its volatility, persistence,

* Corresponding author.
*E-mail address:* nqyan@sjtu.edu.cn (N. Yan).

https://doi.org/10.1016/j.jhazmat.2017.12.016
0304-3894/

bioaccumulation and neurological toxicity [2]. In October 2013, the Minamata Convention on mercury was signed by most countries to prevent Hg emission and release [3]. The components of sintering flue gas is relatively complex due to the use of iron ore, which contains a variety of corrosive gases and heavy metal pollutants (such as: $SO_2$, NOx, dioxin and mercury, et al.). Iron and steel production is considered to be one of the predominant anthropogenic sources of atmospheric mercury (Hg), and the global mercury emissions were estimated to be 46 tons in 2010 [4]. China was the largest iron and steel producer in the world, and made 780 million tons of crude steel in 2013 [4]. Therefore, it is important to control the mercury emissions from iron and steel production.

Previous studies indicated that the mercury emissions from sintering machine accounted for about 90% of total emissions from iron and steel plants [5]. And mercury emitted from sintering flue gas occurred in three forms: elemental mercury ($Hg^0$), oxidized elemental mercury ($Hg^{2+}$), and particle-bound elemental mercury ($Hg^p$). $Hg^0$ was the main form in sintering flue gas [6], which was difficult to remove from flue gas because of its high volatility and low solubility in water compared with $Hg^{2+}$ and $Hg^p$ [5]. Therefore, the mercury removal in sintering flue was mainly the elemental mercury.

Adsorption and oxidation are considered the two main methods for $Hg^0$ removal. And then a large number of adsorbents and catalysts were studied with regard to $Hg^0$ removal by scholars in recent years, such as active carbon, metal oxides and noble metal, etc. [7]. Because the temperature range of sintering flue gas is large, and the content of oxygen and moisture are high, it is necessary to seek a novel adsorbent or catalyst for the $Hg^0$ removal.

Metal-organic frameworks (MOFs) are a novel class of crystalline porous materials, and have recently attracted widespread research interest because of their ultrahigh specific area, ordered crystalline structures, tuneable functionalities, which been employed in gas storage and separation, drug delivery, and heterogeneous catalysis [8]. Generally, MOFs are basically composed of two major components: metal ions or metal cluster occupying nodal positions in a crystalline framework, and the organic units known as linkers or bridging-ligands, such as carboxylates or other organic anions (phosphonate, sulfonate, and heterocyclic compounds) [9].

Regarding their use as heterogeneous adsorbents and catalysts, MOFs offer at least three different possibilities: open metal sites (coordinatively unsaturated), the ligands and large pore volume available. And the most widely explored strategy is to take advantage of the open metal ions as active sites [10]. The open metal sites are built into the pore "walls" in a repeating, regular fashion, which have been shown to impart catalytic activity to the materials. Furthermore, the partial positive charges on the metal sites in MOFs also have the potential to enhance general adsorption properties [11].

Chromium(III) terephthalate (MIL-101(Cr)) is an attractive candidate for the adsorption of gas because of its extra-high specific surface area, large cavities, outstanding thermal and chemical stability [12]. In addition, the presence of chromium clusters not bound to the linkers provides coordinatively unsaturated sites (CUS) with mild Lewis acid properties [13].

There are several reports of MIL-101(Cr) about their implication in adsorption application. Nuzhdin et al. used MIL-101(Cr) to remove nitrogen compounds from liquid hydrocarbon streams, which presented high sorption capacity due to the coordination of nitrogen atoms to the unsaturated $Cr^{3+}$ centres of the MIL-101(Cr) [14]. Leng et al. observed similar interactions during the adsorption of uranine over MIL-101(Cr). The adsorption capacity of uranine over MIL-101-Cr was 126.9 mg/g which was much higher than that of AC(17.5 mg/g) [15]. The $Hg^0$ removal using MOFs has been studied in recent years. Liu et al. found $Hg^0$ stably physi-sorbed on the unsaturated metal center (magnesium ion) of Mg/DOBDC with a binding energy of −27.5 kJ/mol [16]. Zhang et al. synthesized the phenyl bromine-appended metal-organic frameworks (Br-MOFs) and found phenyl bromide on the MOFs was the main active site for $Hg^0$ capture [17]. To our knowledge, there have been few reports regarding MIL-101(Cr) as an adsorbent for the $Hg^0$ removal.

In the paper, MIL-101(Cr) was introduced for the $Hg^0$ removal research. Besides, open-frame-work metal-coordination polymer: $Cu_3(BTC)_2$ (BTC = benzene-1,3,5 -tricarboxylate) [18], and closed packed metal structures: zirconium-based MOF (UiO-66) [19] were selected for the performance comparison. And the physical and chemical properties of the adsorbents, as well as the $Hg^0$ removal efficiency were investigated. Furthermore, the catalytic mechanism involved in removing $Hg^0$ was discussed.

## 2. Experimental

### 2.1. Materials

All chemicals used for adsorbent preparation were of analytical grade. Chromic nitrate nonahydrate ($Cr(NO_3)_3{\cdot}9H_2O$, >99%), 1,4-benzenedicarboxylic acid ($H_2BDC$, 99%), and *N,N′*-dimethylformamide (DMF, 99.5%) were purchased from Aladdin Co. (Shanghai, China); Glacial acetic acid ($CH_3COOH$, >99.5%) were purchased from Shanghai Ling Feng Chemical Reagent Co., Ltd. (Shanghai, China).

### 2.2. Preparation of adsorbents

The synthesis of MIL-101(Cr) was performed using a modified procedure as described in the literature [13]. Generally, $Cr(NO_3)_3{\cdot}9H_2O$ (4.0 g, 10 mmol), terephthalic acid (1.66 g, 10 mmol), and deionized water (60 mL) were blended, and stirred for 1 h at room temperature. Then the suspension was placed in a Teflon-lined autoclave bomb and kept in an oven at 218 °C for 18 h without stirring. After the solution had been cooled to room temperature in air, the resulting solid was centrifuged and washed with DMF and ethyl alcohol for three times at 60 °C, respectively, and finally dried in an oven at 150 °C for 24 h.

Cu-BTC and UiO-66 were synthesized following the procedure reported by Huang et al. [20] and Cavka et al. [19], respectively.

### 2.3. Removal activity evaluation

The $Hg^0$ removal activity of the adsorbents was evaluated in a simulative gas formulating system and reaction device (SHKD-1, Tongsheng Lida Digital Technology Co., Ltd., Beijing), and Tekran 3300 RS online mercury emissions monitoring system. The simulative gas formulating system and reaction device included a fixed-bed reactor (a quartz tube with an inner diameter of 6 mm, and a tube-type resistance furnace) and eight mass-flow controllers to adjust the simulated flue gas compositions. The adsorbent was packed into quartz tube, which was plugged with quartz wool. An $Hg^0$ permeation tube was used to generate $Hg^0$ vapor carried by pure $N_2$, which was then introduced to the inlet of the gas mixer. Tekran 3300 RS online mercury emissions monitoring system detected the total mercury ($Hg^t$) and zero-valent mercury ($Hg^0$) on line. The analytical method employed was cold atomic fluorescence and the enrichment of pure gold amalgam. At the beginning of each test, the gas containing $Hg^0$ was first passed through a bypass without adsorbents. When the concentration of $Hg^0$ had fluctuated within ±5% for more than 30 min, the gas was diverted to pass through the fixed-bed reactor containing the adsorbents. The target Hg concentration of the synthetic flue gas was about 350 μg/m$^3$ and the amount of adsorbent was 20 mg.

Besides, the flow rate of the simulative gas was 500 mL/min, corresponding to a space velocity (SV) of $1.7 \times 10^5$ $h^{-1}$ for $Hg^0$ conversion tests, using $N_2$ as the carrier gas, and the oxygen content was 4%.

The temperature programmed desorption (TPD) curves of Hg were obtained as follows: A known amount of adsorbents were placed in a reaction device with $N_2$ + 4% $O_2$ at 500 mL $min^{-1}$ to adsorb $Hg^0$ for 60 min. Then, the oxygen flow was stopped, and the Hg signal curve was recorded under $N_2$. The heating rate was 5 °C $min^{-1}$, and the temperature range was from 100 °C to 800 °C.

### 2.4. Characterization of the adsorbents

The prepared adsorbents were characterized and analyzed using different techniques. The X-ray diffraction (XRD) patterns of the adsorbents were obtained using an APLX-DUO X-ray diffractometer (BRUKER, Germany) using Cu Kα radiation (40 kV and 20 mA), and the XRD patterns were recorded in a 2θ range from 5 to 70° at a scanning rate of 7° $min^{-1}$. The thermal stabilities of the adsorbents were assessed using a TGA/DSC1 (Mettler Toledo), and the ramp rate for the thermogravimetric analysis (TGA) was 10 °C $min^{-1}$ from 30 to 700 °C. Nitrogen adsorption and desorption isotherms were obtained on a nitrogen-adsorption apparatus (Quantachrome Nova 2200e) at −196 °C. All samples were degassed first for 3 h at 150 °C. Specific surface areas were calculated by use of the Brunauer-Emmett-Teller (BET) method. $H_2$-temperature programmed reduction ($H_2$-TPR) experiments were performed on a Chemisorp TPx 2920 instrument, the sorbents were degassed at 200 °C for 3 h under Ar at atmosphere before $H_2$-TPR test, and the reducing gas was 10% $H_2$/Ar. X-ray photoelectron spectroscopy (XPS) measurements were made using an AXIS UltraDLD(Shimadzu-Kratos) spectrometer with Al Kα radiation as the excitation source. The C1s line at 284.8 eV was taken as a reference for binding energy calibration.

## 3. Results and discussion

### 3.1. Physical and chemical characterization

To identify the crystallographic structure of adsorbents, the XRD patterns of various adsorbents are shown in Fig. 1(a). The diffraction peak positions and relative diffraction intensities of the synthesized adsorbents were in good agreement with some reports and indicated that the adsorbents had been successfully prepared [21–23].

The $N_2$ adsorption-desorption isotherm of adsorbents are shown in Fig. 1(b), and the physical properties calculated from these isotherms are listed in Table 1. The $N_2$ adsorption-desorption isotherm of all adsorbents in Fig. 1(b) were assigned to type IV according to the IUPAC classification and exhibit a type H1 hysteresis at high relative pressure [24]. For the physical properties, all the adsorbents had a large BET surface area and pore volumes in

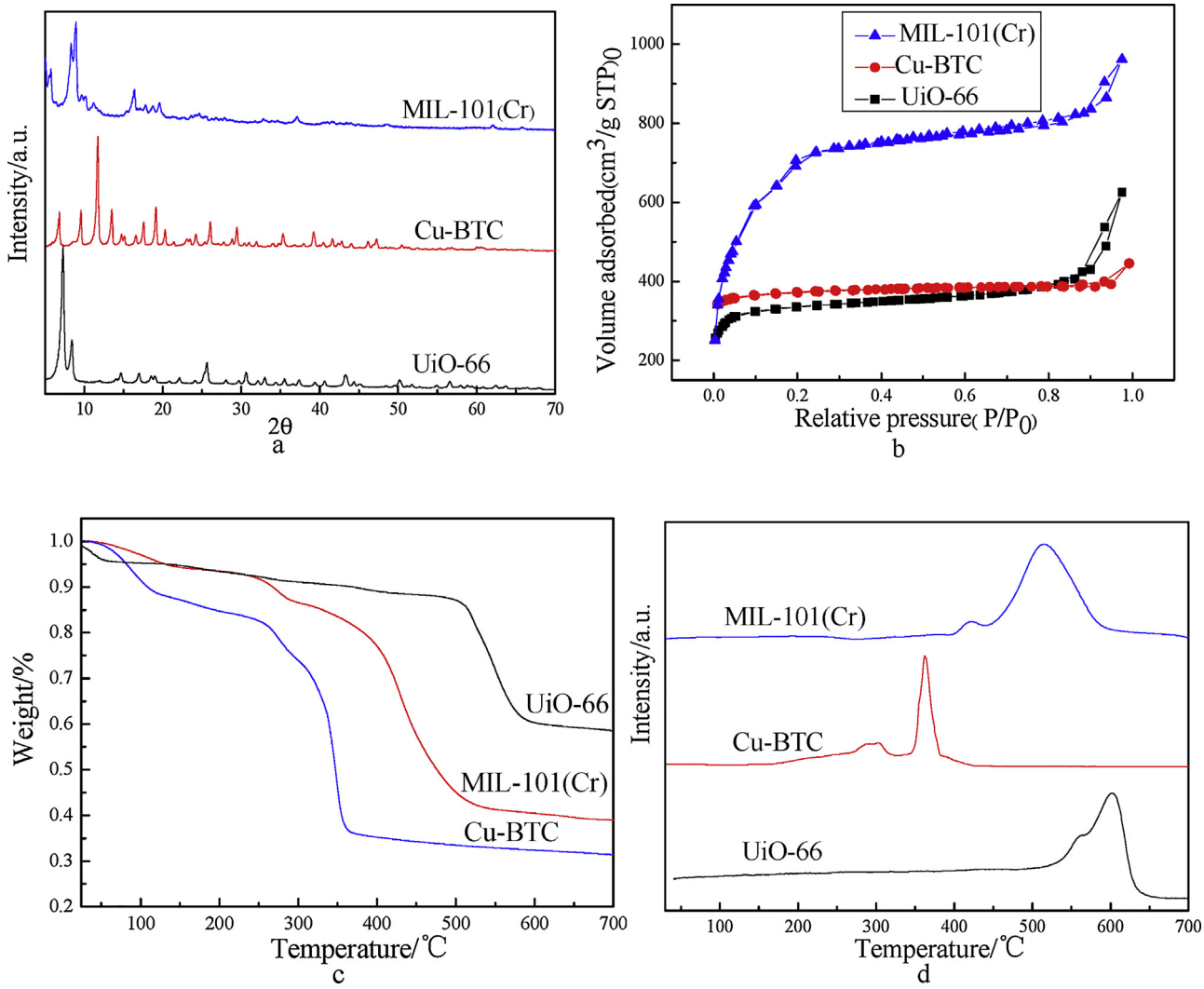


**Fig. 1.** (a) XRD patterns, (b) $N_2$ adsorption-desorption isotherms, (c) TG curves and (d) TPR profiles of various adsorbents.

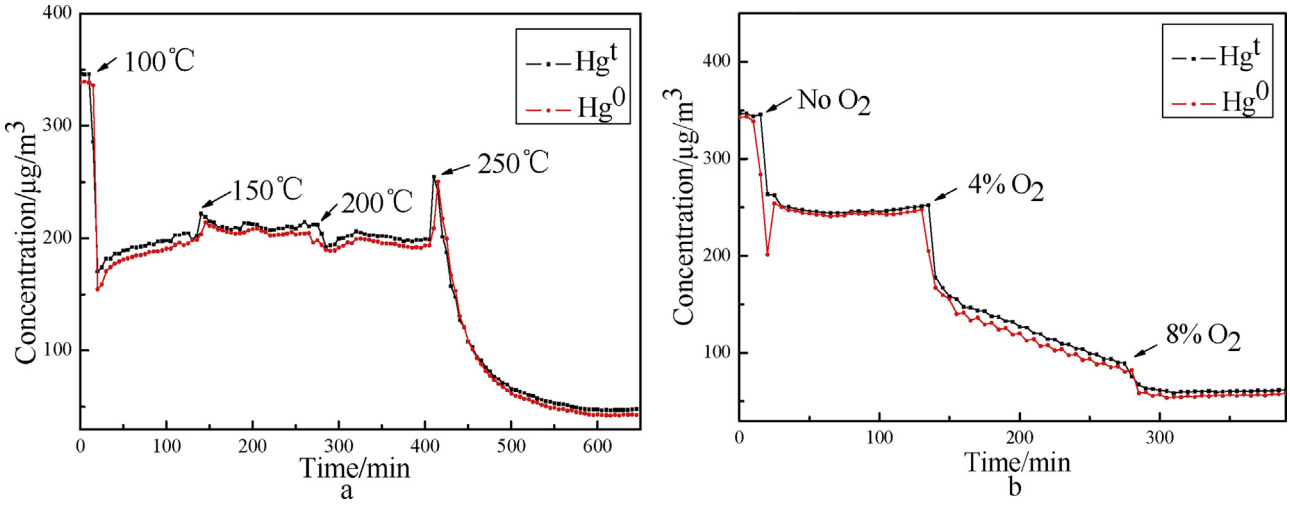


**Fig. 2.** Elemental mercury and total mercury concentration change curves passing through MIL-101(Cr): (a) temperature effect, (b) oxygen content effect.

**Table 1**
BET surface areas and pore volumes of various adsorbents ($m^2$ /g).

| Sample | UiO-66 | Cu-BTC | MIL-101(Cr) |
|---|---|---|---|
| $S_{BET}$ ($m^2$/g) | 1090.672 | 1189.662 | 2487.940 |
| Pore Volume (cc/g) | 0.941 | 0. 533 | 0.755 |

Table 1, while MIL-101(Cr) had the largest BET surface area, which was beneficial for adsorbing reaction components.

Thermogravimetric (TG) analysis was performed to assess the thermal stability of the adsorbents, as shown in Fig. 1(c). The weight loss of all adsorbents occurred mainly at three temperature phase. The weights loss of the adsorbents below 100 °C may be attributed to the loss of physically adsorbed water and solvent molecules. And the weight loss between 100 °C and 300 °C for MIL-101(Cr) and Cu-BTC was due to organic residues, while the temperature lasting until 500 °C for UiO-66. It indicated that MIL-101(Cr), Cu-BTC and UiO-66 had high thermal stability, and could be used for $Hg^0$ removal under 300 °C. The maximum decomposition temperatures for MIL-101(Cr), Cu-BTC and UiO-66 were approximately 300, 400 and 500 °C, respectively, which may be due to the breakdown of the organic framework. In brief, prepared MOFs adsorbents had high thermal stability.

Fig. 1(d) shows the temperature-programmed reduction (TPR) profiles of the different adsorbents. There is a broad reduction peak starting from 520 °C and ending at 630 °C for UiO-66. The shoulder peak at 550 °C might originate from oxygen species released from the inner structure, and the maxima at 600 °C could be attributed to the reduction of zirconium oxides [25,26]. The $H_2$-TPR profile for Cu-BTC shows two reduction features, the peak at approximately 280 °C is attributed to $Cu^{2+}$ of the open metal site, and the peak at approximately 350 °C can be ascribed for the $Cu^{2+}$ connected to the ligand due to the breakdown of the organic framework [27]. Similarly, MIL-101(Cr) also presents two the reduction peaks, indicates that it has a certain oxidation capacity. The peak at approximately at 420 is due to $Cr^{3+}$ of the open metal site, and the peak at approximately 500 °C can be attributed to connected $Cr^{3+}$ because of the breakdown of the organic framework [28], these results were consistent with that of TG analysis.

### 3.2. $Hg^0$ removal performance

Fig. 2 shows the elemental mercury and total mercury concentration change curves passing through MIL-101(Cr) at different temperatures and oxygen content. As can be seen from Fig. 2(a),

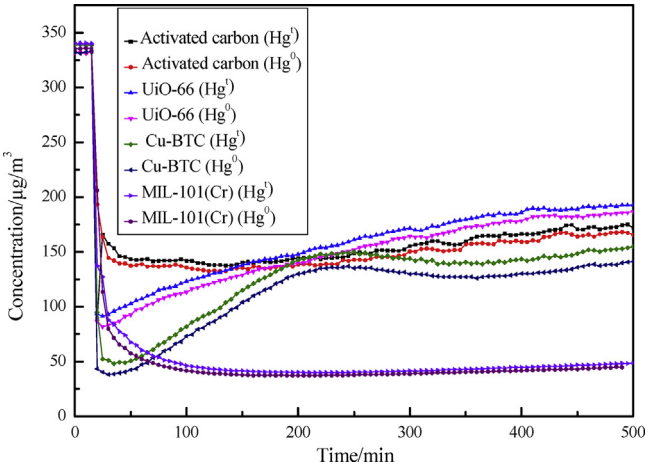


**Fig. 3.** Elemental mercury and total mercury concentration change curves passing through various adsorbents at 250 °C.

when $Hg^0$ was passed through adsorbents, both $Hg^0$ and $Hg^t$ concentration presented decreased, and the difference value between elemental mercury and total mercury did not change with the increasing time, indicated that no divalent mercury entered into flue gas. Furthermore, the $Hg^0$ removal efficiency increased with the increasing temperature, manifested that the performance of MIL-101(Cr) was better at higher temperature. Fig. 2(b) shows the oxygen content effect on the $Hg^0$ removal. MIL-101(Cr) still had $Hg^0$ removal ability when no $O_2$ was present, which might be due to the open metal site $Cr^{3+}$. While the $Hg^0$ removal efficiency decreased with the increasing time, indicated that the open metal site was consumed and did not recover. When 4% $O_2$ was added, the $Hg^0$ removal efficiency of MIL-101(Cr) increased significantly, indicating that the additional oxygen enhanced the performance of adsorbent, which might be because the open metal site was reactivated by added $O_2$. Continuing to increase the oxygen content, the promotion of $Hg^0$ removal efficiency of MIL-101(Cr) was little, manifesting that 4% $O_2$ was sufficient in the adsorbent reaction.

Fig. 3 shows the elemental mercury and total mercury concentration change curves passing through various adsorbents at 250 °C. The difference value for total mercury ($Hg^t$) and elemental mercury ($Hg^0$) is the amount of divalent mercury ($Hg^{2+}$). It can be seen from Fig. 3 that the concentrations of $Hg^t$ and $Hg^0$ both decreased after passing through adsorbents. However, there was very little divalent

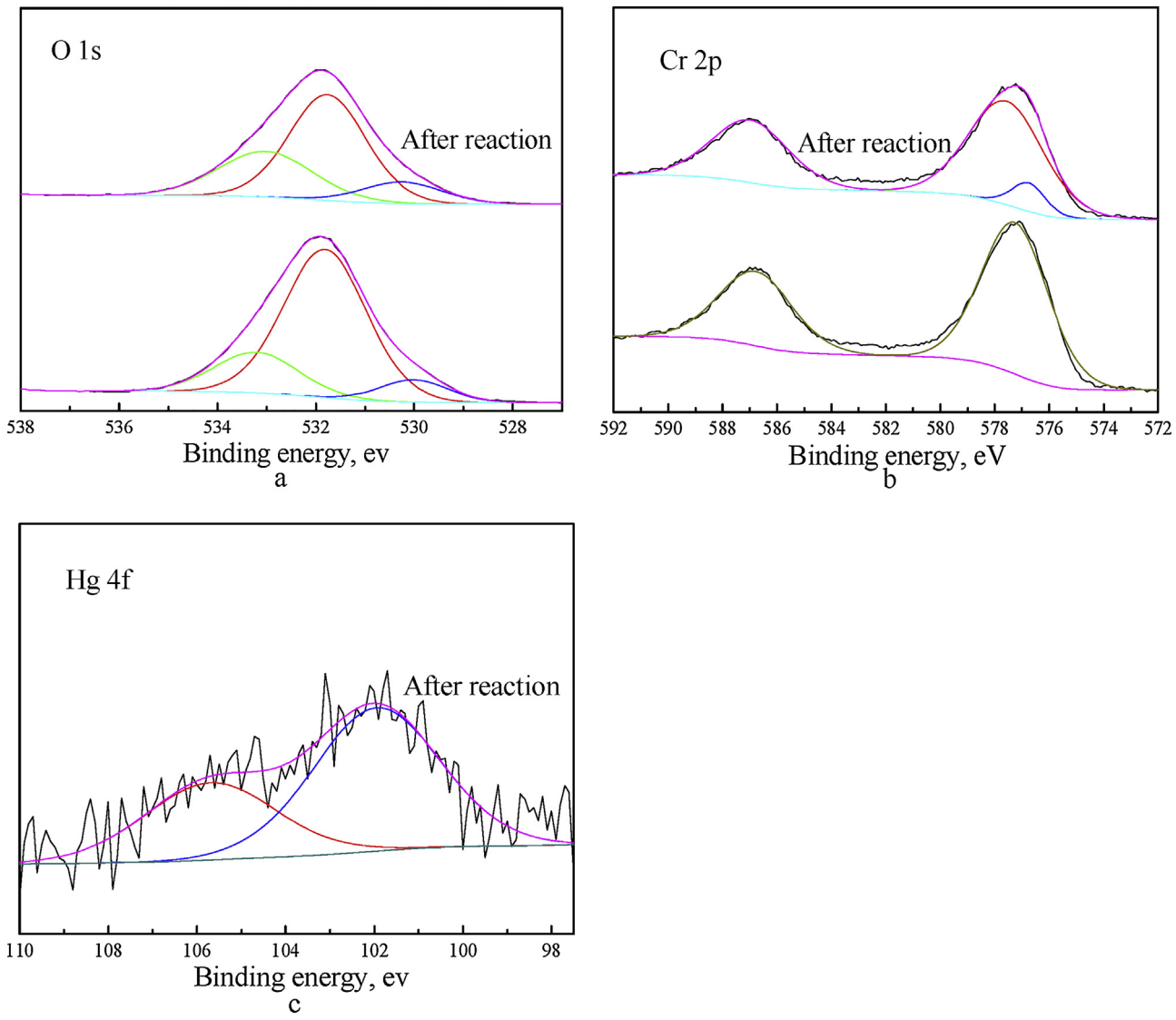


**Fig. 4.** XPS spectra of MIL-101(Cr) over the O 1s, Cr 2p and Hg 4f spectral regions.

mercury in flue gas, indicating that $Hg^0$ was captured by adsorbents or the generated $Hg^{2+}$ combined with adsorbent. Furthermore, Mil-101(Cr) had the highest $Hg^0$ removal efficiency compared with UiO-66, Cu-BTC and activated carbon, indicated that the open metal site $Cr^{3+}$ was more active than that of UiO-66 and Cu-BTC.

### 3.3. $Hg^0$ removal mechanism over MIL-101(Cr)

#### 3.3.1. XPS analysis

Fig. 4 shows the XPS spectra of MIL-101(Cr) over the O 1s, Cr 2p and Hg 4f spectral regions before and after reaction. And the percent of valence state for O 1s, Cr 2p and Hg 4f is shown in Table 2.

The O 1s XPS spectrum of MIL-101(Cr) can be deconvoluted into three peaks. The peak at 529.8 eV can be ascribed to lattice oxygen due to Cr—O bonds, and the peak at 531.6 eV can be attributed to surface chemisorbed oxygen. Furthermore, the peak at approximately 533.1 eV can be attributed to oxygen components of the carboxylate groups [19]. After reaction at 200 °C, the proportion of surface chemisorbed oxygen decreases markedly, indicating that the chemisorbed oxygen participates in the process of $Hg^0$ removal, which is an active component for $Hg^0$ removal.

There are two obvious photoelectron peaks for the chromium 2p3/2 and 2p1/2 with the centers at 576.9 and 586.7 eV, respectively, which are attributed to $Cr^{3+}$ [29]. After reaction, the intensity of the Cr 2p peaks is weaker, which might be due to the combination effect with Hg. Furthermore, an additional peak at approximately at 576.2 eV can be found, which can be assigned to $Cr^{2+}$ [30]. This indicated that the open metal chromium would oxidize $Hg^0$ and then change to lower valence state itself. In the presence of oxy-

**Table 2**
Percent of valence state at different binding energy.

| | O 1s | | | Cr 2p | | | Hg 4f | |
|---|---|---|---|---|---|---|---|---|
| Binding energy (eV) | 530 | 531.8 | 533.2 | 576.2 | 577.2 | 586.8 | 101.9 | 105.6 |
| Percent of valence state (%) | 8.88 | 71.26 | 19.86 | 0 | 64.74 | 35.26 | | |
| Percent of valence state (%) (after reaction) | 12.19 | 57.56 | 30.25 | 7.22 | 57.28 | 35.5 | 63.87 | 36.13 |

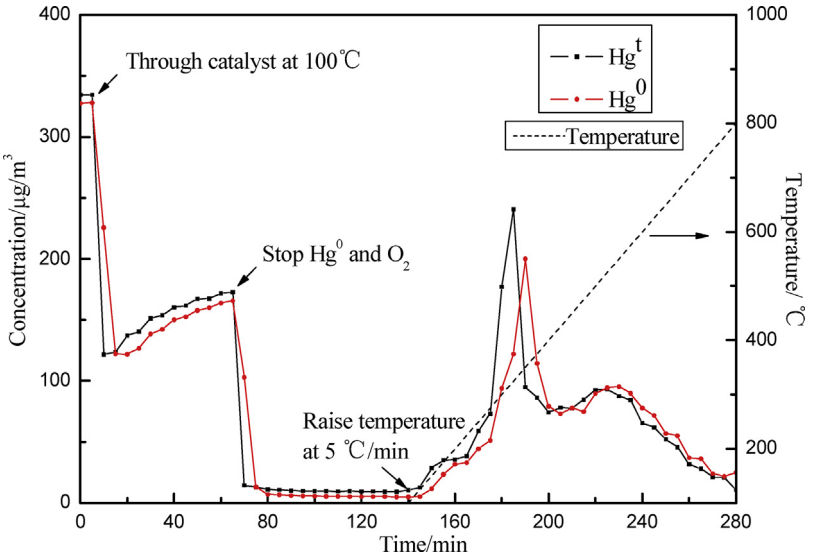


**Fig. 5.** The $Hg^0$ adsorption and desorption curve of Mil-101(Cr).

**Table 3**
$Hg^0$ amount of adsorption and desorption for 1 h at 100 °C.

| | adsorption | desorption | trapping percent (%) |
|---|---|---|---|
| $Hg^0$ amount (mg/g) | 0.249 | 0.237 | 95.18 |

gen, the $Cr^{2+}$ could be oxidized to $Cr^{3+}$ again by the oxygen. The analysis is consistent with Fig. 2(b).

Fig. 4(C) shows the Hg 4f XPS patterns. As can be found in Fig. 4(c), the Hg 4f region is deconvoluted into two peaks with centers at approximately101.5 eV and 105.5 eV, which is attributed to the mercuric oxide (HgO) species [31,32], indicating that $Hg^0$ is oxidized over MIL-101(Cr) and remained on the surface of adsorbent.

### 3.3.2. *The analysis of $Hg^0$ desorption*

To study the Hg combination properties of the adsorbents, $Hg^0$ adsorption and desorption experiments were performed, shown in Fig. 5. Mil-101(Cr) adsorbed $Hg^0$ for 1 h. Then, $Hg^0$ and oxygen were stopped, and nitrogen purged the adsorbent to wipe off weak adsorbed $Hg^0$ on the surface of adsorbent. Finally, Hg signal curve was recorded at a heating rate of for 5 °C $min^{-1}$ from 100 °C to 800 °C. It can be seen from Fig. 5 that $Hg^0$ started to release from 100 °C to 250 °C, which was assigned to chemical adsorption of mercury on the surface of adsorbent. And $Hg^0$ presented a sharply increase around 300 °C, which might be due to the structural decomposition referring to the results of TG and XPS. Furthermore, $Hg^0$ releasing at approximately 400 °C and ending at approximately 800 °C was attributed to the release chemical adsorption of mercury inside MiL-101(Cr), which might because of the structural decomposition referred to the result of TG and XPS. Base on the integral calculation, the $Hg^0$ amount of adsorption and desorption for 1 h at 100 °C is shown in Table 3. The adsorbed $Hg^0$ was 0.249 mg/g, and the desorbed $Hg^0$ was 0.237 mg/g, indicating that almost all of the adsorbed $Hg^0$ existed on Mil-101(Cr), which showed a good combining ability for chemisorbed mercury.

### 3.3.3. *The main reaction pathway*

Based on these results, a plausible mechanism for $Hg^0$ removal is proposed as follows:

$Hg^0$ was first adsorbed on the surface of Mil-101(Cr), which was oxidized by the open metal site $Cr^{3+}$. The $Cr^{2+}$ was then oxidized to $Cr^{3+}$ again by surface active oxygen of adsorbent, and the generated $Hg^{2+}$ combined adsorbed oxygen to generate HgO.

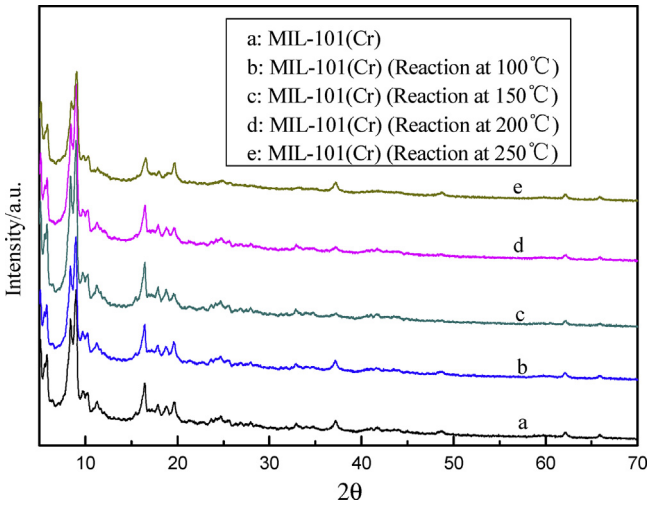


**Fig. 6.** The XRD patterns of MIL-101(Cr) after reaction at different temperatures.

$$Hg^0(g) \rightarrow Hg^0(ads) \quad (1)$$

$$2MIL\text{-}101(Cr^{3+}) + Hg^0(ads) \rightarrow 2MIL\text{-}101(Cr^{2+}) + Hg^{2+}(ads) \quad (2)$$

$$2MIL\text{-}101(Cr^{2+}) + O(sur) \rightarrow 2MIL\text{-}101(Cr^{3+}) + O^{2-}(sur) \quad (3)$$

$$Hg^{2+}(ads) + O^{2-}(sur) \rightarrow HgO(ads) \quad (4)$$

### 3.3.4. *The stability analysis*

To investigate the chemical and thermal stability of MIL-101(Cr), XRD patterns after reaction were recorded at different temperatures. The results (Fig. 6) show that all diffraction peak positions had not changed and relative intensities were still strong. This indicated that the structure and crystal form were not destroyed after reaction, and MIL-101(Cr) had good chemical and thermal stability.

## 4. Conclusions

In summary, MIL-101(Cr) was prepared successfully. The physical and chemical characterization of the adsorbents showed that MIL-101(Cr) had the largest BET surface area, high thermal sta-

bility and oxidation capacity. $Hg^0$ removal performance analysis indicated that the $Hg^0$ removal efficiency of MIL-101(Cr) increased with the increasing temperature and oxygen content, and MIL-101(Cr) had the highest $Hg^0$ removal performance compared with Cu-BTC, UiO-66 and activated carbon. The $Hg^0$ removal mechanism was analyzed by XPS and Hg-TPD, manifested that $Hg^0$ was first adsorbed on the surface of Mil-101(Cr), and then oxidized by the open metal site $Cr^{3+}$. The surface adsorbed oxygen of adsorbent combined with generated $Hg^{2+}$ to generate HgO, and oxidized the open metal site $Cr^{2+}$ to $Cr^{3+}$. Furthermore, MIL-101(Cr) had good chemical and thermal stability.

## Acknowledgements

This study was supported by the National Key Research and Development Program of China (No. 2017YFC0210502) and the National Natural Science Foundation of China (No. 21677096) and (No. 21607102), and China's Post-doctoral Science Fun (No. 2015M581626).

## References

[1] S. Zhao, Y. Ma, Z. Qu, N. Yan, Z. Li, J. Xie, W. Chen, The performance of Ag doped $V_2O_5$-$TiO_2$ catalyst on the catalytic oxidation of gaseous elemental mercury, Catal. Sci. Technol. 4 (2014) 4036–4044.
[2] Y. Gao, Z. Zhang, J. Wu, L. Duan, A. Umar, L. Sun, Z. Guo, Q. Wang, A critical review on the heterogeneous catalytic oxidation of elemental mercury in flue gases, Environ. Sci. Technol. 47 (2013) 10813–10823.
[3] S. Zhao, Z. Qu, N. Yan, Z. Li, H. Xu, J. Mei, F. Quan, The performance and mechanism of Ag-doped $CeO_2$ /$TiO_2$ catalyst on the catalytic oxidation of gaseous elemental mercury, Catal. Sci. Technol. 5 (2015) 2985–2993.
[4] F. Wang, S. Wang, Z. Lei, Y. Hai, G. Wei, Q. Wu, J. Hao, Mercury mass flow in iron and steel production process and its implications for mercury emission control, J. Environ. Sci. 43 (2016) 293–301.
[5] N. Fukuda, M. Takaoka, S. Doumoto, K. Oshita, S. Morisawa, T. Mizuno, Mercury emission and behavior in primary ferrous metal production, Atmos. Environ. 45 (2011) 3685–3691.
[6] D.G. Streets, J. Hao, Y. Wu, J. Jiang, M. Chan, H. Tian, X. Feng, Anthropogenic mercury emissions in China, Atmos. Environ. 39 (2005) 7789–7806.
[7] S. Zhao, Z. Li, Z. Qu, N. Yan, W. Huang, W. Chen, H. Xu, Co-benefit of Ag and Mo for the catalytic oxidation of elemental mercury, Fuel 158 (2015) 891–897.
[8] Z. Xu, C.L. Xu, L. Yang, Pt@UiO-66 heterostructures for highly selective detection of $H_2O_2$ with an extended linear range, Anal. Chem. 87 (2015) 3438–3444.
[9] H. Zubair, J. Sung Hwa, Removal of hazardous organics from water using metal-organic frameworks (MOFs): plausible mechanisms for selective adsorptions, J. Hazard. Mater. 283 (2015) 329.
[10] A. Dhakshinamoorthy, H. Garcia, Catalysis by metal nanoparticles embedded on metal-organic frameworks, Chem. Soc. Rev. 41 (2012) 5262–5284.
[11] J.R. Karra, K.S. Walton, Effect of open metal sites on adsorption of polar and nonpolar molecules in metal−organic framework Cu-BTC, Langmuir 24 (2008) 8620–8626.
[12] X. Sun, Y. Li, H. Xi, Q. Xia, Adsorption performance of a MIL-101(Cr)/graphite oxide composite for a series of n-alkanes, RSC Adv. 4 (2014) 56216–56223.
[13] L. Bromberg, Y. Diao, H. Wu, S.A. Speakman, T.A. Hatton, Chromium(III) terephthalate metal organic framework (MIL-101): HF-free synthesis, structure, polyoxometalate composites, and catalytic properties, Chem. Mater. 24 (2012) 1664–1675.
[14] A.L. Nuzhdin, K.A. Kovalenko, D.N. Dybtsev, G.A. Bukhtiyarova, Removal of nitrogen compounds from liquid hydrocarbon streams by selective sorption on metal-organic framework MIL-101, Mendeleev Commun. 20 (2010) 57–58.
[15] F. Leng, W. Wang, X.J. Zhao, X.L. Hu, Y.F. Li, Adsorption interaction between a metal–organic framework of chromium–benzenedicarboxylates and uranine in aqueous solution, Colloids Surf. A Physicochem. Eng. Aspects 441 (2014) 164–169.
[16] Y. Liu, H. Li, J. Liu, Theoretical prediction the removal of mercury from flue gas by MOFs, Fuel 184 (2016) 474–480.
[17] X. Zhang, B. Shen, S. Zhu, H. Xu, L. Tian, UiO-66 and its Br-modified derivates for elemental mercury removal, J. Hazard. Mater. 320 (2016) 556.
[18] S. Liu, L. Sun, F. Xu, J. Zhang, C. Jiao, F. Li, Z. Li, S. Wang, Z. Wang, X. Jiang, Nanosized Cu-MOFs induced by graphene oxide and enhanced gas storage capacity, Energy Environ. Sci. 6 (2013) 818–823.
[19] J.H. Cavka, S. Jakobsen, U. Olsbye, N. Guillou, C. Lamberti, S. Bordiga, K.P. Lillerud, A new zirconium inorganic building brick forming metal organic frameworks with exceptional stability, J. Am. Chem. Soc. 130 (2008) 13850–13851.
[20] W. Huang, X. Zhou, Q. Xia, J. Peng, H. Wang, Z. Li, Preparation and adsorption performance of GrO@Cu-BTC for separation of $CO_2$/$CH_4$, Ind. Eng. Chem. Res. 53 (2014) 11176–11184.
[21] A. Grzech, J. Yang, T.J. Dingemans, S. Srinivasan, P.C.M.M. Magusin, F.M. Mulder, Irreversible high-temperature hydrogen interaction with the metal organic framework $Cu_3(BTC)_2$, J. Phys. Chem. C 115 (2011) 21521–21525.
[22] Z. Hasan, J.W. Jun, S.H. Jhung, Sulfonic acid-functionalized MIL-101(Cr): an efficient catalyst for esterification of oleic acid and vapor-phase dehydration of butanol, Chem. Eng. J. 278 (2015) 265–271.
[23] W. Dong, C. Feng, Z. Li, N. Shang, S. Gao, C. Wang, Z. Wang, Pd@UiO-66: an efficient catalyst for Suzuki–Miyaura coupling reaction at mild condition, Catal. Lett. 146 (2016) 1–9.
[24] Z. Yu, J. Deschamps, L. Hamon, P.K. Prabhakaran, P. Pré, Hydrogen adsorption and kinetics in MIL-101(Cr) and hybrid activated carbon-MIL-101(Cr) materials, Int. J. Hydrogen Energy 42 (2017) 8021–8031.
[25] V. Idakiev, T. Tabakova, K. Tenchev, Z.Y. Yuan, T.Z. Ren, B.L. Su, Gold catalysts supported on ceria-modified mesoporous zirconia for low-temperature water–gas shift reaction, J. Porous Mater. 19 (2012) 15–20.
[26] J. Ouyang, H. Yang, Enhanced reduction properties of mesostructured $Ce_{0.5}Zr_{0.5}O_2$ solid solutions, Mater. Chem. Phys. 140 (2013) 294–299.
[27] D.W. Jeong, H.S. Na, J.O. Shim, W.J. Jang, H.S. Roh, U.H. Jung, L.Y. Wang, Hydrogen production from low temperature WGS reaction on co-precipitated Cu–$CeO_2$ catalysts: An optimization of Cu loading, Int. J. Hydrogen Energy 39 (2014) 9135–9142.
[28] H. Zhao, H. Song, L. Chou, Synthesis and catalytic application in isobutane dehydrogenation of the mesoporous chromia/alumina catalysts based on a metal–organic framework, Microporous Mesoporous Mater. 181 (2013) 182–191.
[29] X. Li, J. Cao, W. Zhang, Stoichiometry of Cr (VI) immobilization using nanoscale zerovalent iron (nZVI): a study with high-resolution X-ray photoelectron spectroscopy (HR-XPS), Ind. Eng. Chem. Res. 47 (2008) 2131–2139.
[30] Z. Chen, Q. Yang, H. Li, X. Li, L. Wang, S.C. Tsang, Cr–$MnO_x$ mixed-oxide catalysts for selective catalytic reduction of $NO_x$ with $NH_3$ at low temperature, J. Catal. 276 (2010) 56–65.
[31] Z.S. Wei, Y.W. Luo, B.R. Li, Z.Y. Chen, Q.H. Ye, Q.R. Huang, J.C. He, Elemental mercury oxidation from flue gas by microwave catalytic oxidation over Mn/γ-$Al_2O_3$, J. Ind. Eng. Chem. 24 (2015) 315–321.
[32] G.W. Wu, S.B. He, H.P. Peng, H.H. Deng, A.L. Liu, X.H. Lin, X.H. Xia, W. Chen, Citrate-capped platinum nanoparticle as a smart probe for ultrasensitive mercury sensing, Anal. Chem. 86 (2014) 10955–10960.